



Contents lists available at ScienceDirect

Spectrochimica Acta Part A: Molecular and Biomolecular Spectroscopy

journal homepage: www.elsevier.com/locate/saa

Assessment of conformational, spectral, antimicrobial activity, chemical reactivity and NLO application of Pyrrole-2,5-dicarboxaldehyde bis(oxaloyldihydrazone)



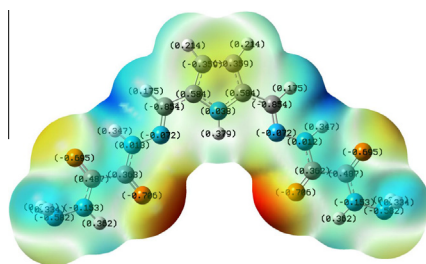
Poonam Rawat, R.N. Singh*

Department of Chemistry, University of Lucknow, Lucknow 226007, U.P., India

HIGHLIGHTS

- Solid state FT-IR spectrum characterization of PDBO.
- Experimental and calculated spectroscopic analysis confirm the formation of product.
- The calculated first hyperpolarizability (β_0) value of PDBO is 23.83×10^{-30} esu.
- Antimicrobial efficiency of PDBO was analyzed by "Disc Diffusion Assay".

GRAPHICAL ABSTRACT



ARTICLE INFO

Article history:

Received 30 July 2014

Received in revised form 15 December 2014

Accepted 17 December 2014

Available online 25 December 2014

Keywords:

Hydrogen bond

NBO analysis

QTAIM calculation

Reactivity descriptors

ABSTRACT

An orange colored pyrrole dihydrazone: Pyrrole-2,5-dicarboxaldehyde bis(oxaloyldihydrazone) (PDBO) has been synthesized by reaction of oxalic acid dihydrazide with 2,5 diformyl-1H-pyrrole and has been characterized by spectroscopic analysis (^1H , ^{13}C NMR, UV-visible, FT-IR and DART Mass). The properties of the compound has been evaluated using B3LYP functional and 6-31G(d,p)/6-311+G(d,p) basis set. The symmetric (3319 , 3320 cm^{-1}) and asymmetric (3389 , 3382 cm^{-1}) stretching wave number confirm free NH_2 groups in PDBO. NBO analysis shows, inter/intra molecular interactions within the molecule. Topological parameters have been analyzed by QTAIM theory and provide the existence of intramolecular hydrogen bonding ($\text{N}-\text{H} \cdots \text{O}$). The local reactivity descriptors analyses determine the reactive sites within molecule. The calculated first hyperpolarizability value ($\beta_0 = 23.83 \times 10^{-30}$ esu) of pyrrole dihydrazone shows its suitability for non-linear optical (NLO) response. The preliminary bioassay suggested that the PDBO exhibits relatively good antibacterial and fungicidal activity against *Escherichia coli*, *Pseudomonas aeruginosa*, *Staphylococcus aureus*, *Streptococcus pyogenes*, *Candida albicans*, *Aspergillus niger*. The local reactivity descriptors – Fukui functions (f_k^+ , f_k^-), local softnesses (s_k^+ , s_k^-) and electrophilicity indices (ω_k^+ , ω_k^-) analyses have been used to determine the reactive sites within molecule.

© 2014 Elsevier B.V. All rights reserved.

Introduction

The chemistry of polyfunctional metal complexes has become a fascinating area of research in contemporary coordination chemistry following the discovery of multinuclear sites in several

enzymes [1] and development of novel functional materials showing molecular ferromagnetism [2] and specific catalytic properties [3]. Heteroatoms influence various properties of material and their applications [4–6].

Mono- and bishydrazones find wide application in medicine as active physiological preparations, due to their antibacterial, tuberculostatic, fungicidal properties as well as activities against certain types of cancers. The dihydrazones are capable of giving rise to

* Corresponding author. Tel.: +91 9451308205.

E-mail address: rnsvk.chemistry@gmail.com (R.N. Singh).

monometallic [7], homobimetallic [8] and heterobimetallic [9] complexes. Bis-acylhydrazones and their metal complexes have attracted great and growing interest due to chemical properties, therapeutic activity, biological significance, industrial importance and structural variety and Fe overload disease. They have also been used as fluorescent materials, pigments, analytical reagents and polymer-coating [10]. Bis-acylhydrazones held a special place in the field of hydrazone chemistry [11] due to (i) the presence of two coordinating unit in these ligands may yield supramolecular architectures or better coordinative properties than those a sole coordinative unit, (ii) a ditopic ligand enables the properties of its complexes to be modulated by the degree of deprotonation, and (iii) Metal complexes of dihydrazones may be able to mimic bimetallic sites in various enzymes. The biocidal properties of dihydrazones dependent on the organic group and the ligand attached to metal [11].

Previously, wide series of hydrazones of 2-formylpyrrole have been synthesized and studied [12–15], while the data on bis-hydrazones of 2,5-diformylpyrrole are extremely rare [16–18]. However, less attention has been paid to synthesis, metal complexes or organometallic complexes with diacylhydrazones as multidentate ligands of diformyl pyrrole [19].

Organic materials are molecular materials that consist of chemically bonded molecular units interacting in the bulk media through weak van-der Waal interactions and possess ease of fabrication and integration into devices, relatively low cost, fast response, intrinsic tailorability which is responsible for NLO properties [20,21]. NLO materials have gained attention in recent years with respect to their future potential applications in the field of optoelectronic such as optical communication, optical computing, optical switching and dynamic image processing [22]. The vibrational spectral studies of the molecule can provide deeper knowledge about the relationships between molecular architecture, nonlinear response and hyperpolarizability.

As per literature survey synthesis and study on pyrrole dihydrazones of oxalic acid dihydrazide were not found reported. The interest, therefore, arouse in this work. The objectives of the present investigation are synthesis, structural elucidation, spectral characterization, evaluation of NLO properties and chemical reactivity. In addition to this antimicrobial activity of PDBO has also been evaluated against antibacterial (*Escherichia coli*, *Pseudomonas aeruginosa*, *Staphylococcus aureus*, *Streptococcus pyogenes*) and fungal (*Candida albicans*, *Aspergillus niger*) species. In this study molecular parameters have been computed using B3LYP functional and 6-311+G(d,p) basis set. This method predicts relatively accurate molecular structure with moderate computational effort. The calculated FT-IR spectrum was analyzed on the basis of the potential energy distribution (PED) of each vibrational mode, which allowed obtaining a quantitative as well as qualitative interpretation of the infrared spectrum. In addition to this, weaker interactions and intramolecular charge transfer has been studied with the help of Quantum theory of Atoms in Molecules (QTAIM) [23] and Natural bond analysis (NBO), respectively.

Experimental details

Synthesis of Pyrrole-2,5-dicarboxaldehyde bis(oxaloyldihydrazone) (5 = PDBO)

2,5-diformyl-1H-pyrrole [24] (0.1000 gm, 0.47 mmol) and oxalic acid dihydrazide (0.1110 gm, 0.94 mmol) were dissolved in methanol and water by ($v/v = 1/3$) solution. The above mixture was allowed to stir for 4 h. The color of the solution changes to orange and completion of reaction was analyzed using thin layer chromatography (TLC). TLC analysis was carried out using glass

plates pre-coated with silica gel (Kieselgel 60 F256, 0.2 mm, Merck). The product was separated by column chromatography on silica using hexane and ethylacetate as eluent. Thus pure orange color product was obtained along with other side products. Yield: 60.41%, Melting point: decompose above 243 °C. UV-visible (DMSO, $c = 10^{-5}$ mol dm⁻³): Elemental Analysis: for C₁₀H₁₃N₉O₄ calcd. C, 37.15; H, 4.05; N, 39.00; Obs. C, 37.45; H, 4.09; N, 39.08; MS (DART) for C₁₀H₁₃N₉O₄: calcd. $m/z = 323.10$, obs. $m/z = 324.20$ (M+H⁺).

Synthesis of macrocyclic bis-hydrazone of pyrrole (6)

The reaction mixture of 2,5 diformyl-1H-pyrrole (0.100 g, 1.219 mmol) and oxalic acid dihydrazide (0.0498 g, 1.219 mmol) in ratio 1:1 were taken in methanol with small amount of conc. HCl. The reaction was refluxed for eight hour, orange color precipitate was obtained. Color: Orange, Yield: 58%. Solubility: Poor solubility in organic solvents. Elemental analysis, ¹H NMR and Mass spectra of the formed macrocyclic bis-hydrazone (6) are reported as: Elemental analysis for C₁₆H₁₄N₁₀O₄ calc. C, 46.83; H, 3.44; N, 34.13; obs. C 46.79, H 3.41, N 34.13. ¹H NMR (300 MHz, DMSO-_{d6}): δ 11.623 (s, 2H, pyrrolic NH), 11.049 (s, 4H, hydrazone-NH), 8.884 (s, 4H, azomethine CH=N-), 6.396–6.369 (4H, pyrrolic ring CH). The MS for C₁₆H₁₄N₁₀O₄ calc. 410.12 amu, found m/z 411 [M+H⁺].

Quantum chemical calculations

The structure of the compound was drawn on Chemdraw ultra 3D software and the quantum chemical calculations were carried out with Gaussian 03 program package [25] to predict the molecular structure, ¹H NMR chemical shifts, vibrational wavenumbers and energies of the optimized structures using DFT(B3LYP) method and 6-31G(d,p), B3LYP/6-311+G(d,p) basis set [26,27]. All the molecular structures are visualized using software Gauss-view [28]. Internal coordinate system recommended by Pulay et al. [29] is used for the assignment of vibrational modes. Potential energy distribution along internal coordinates is calculated by Gar2ped software [30]. The topological properties at the BCPs have been calculated by using the Bader's theory of 'Atoms in Molecules (AIM), implemented in AIM 2000 software [31].

Evaluation of antimicrobial activity

The antimicrobial activity has been study with the help of disc plate diffusion assay procedures. The compound (PDBO), reactant: 2,5-diformyl-1H-pyrrole and oxalic acid dihydrazide were dissolved in DMSO. Proper drug Chloramphenicol and Nystatin were used as control. All compound and reactants were taken at concentration of 100 and 200 μ g/ml for testing antibacterial activity and antifungal activity. The compounds diffused into the medium produced a concentration gradient. After the incubation period, the zones of inhibition were measured in mm. The tabulated results represent the actual readings control. The compound was tested against *E. coli*, *P. aeruginosa* (gram negative bacteria), *S. aureus*, *S. pyogenes* (gram positive bacteria), *C. albicans* and *A. niger* (fungi). The plates were placed in an incubator at 37 °C within 30 min of preparation for bacteria and 22 °C for fungal. After 48 h incubation for bacteria and 7-days for fungal, the diameter of zone (including the diameter disc) was measured and recorded in mm. The measurements were taken with a ruler, from the bottom of the plate, without opening the lid.

Result and discussion

Depending on ratio of reactants 2,5-diformyl-1*H*-pyrrole (4) and oxalic acid dihydrazide (3) as well as used solvents and reaction conditions, the products such as Pyrrole-2,5-dicarboxaldehyde bis(oxaloyldihydrazone), macrocycle and polymeric products were formed [18]. The general route for synthesis of PDBO (5) and (6) are shown in [Supplementary Scheme S1](#). When 2,5-diformyl-1*H*-pyrrole react with oxalic acid dihydrazide in a stoichiometric ratio of 1:2, compound Pyrrole-2,5-dicarboxaldehyde bis(oxaloyldihydrazone) (5 = PDBO), is formed as major product along with (6) as minor. The compound (5 = PDBO) was orange in color, stable and stored at room temperature for longer period of time. The compound decomposes above 243 °C without melting. If 2,5-diformyl-1*H*-pyrrole was reacted with oxalic acid dihydrazide in stoichiometric ratio of 1:1, at higher temperature macrocyclic bis-hydrazone (6) was obtained. The macrocyclic bis-hydrazone (6) has poor solubility in most of the organic solvents. Therefore, the spectral analysis, biological activity and all quantum chemical calculations have been performed on PDBO compound.

Conformational and topological analysis

The molecular geometry and conformational analysis plays a very important role in determining the structure–activity relationship [32]. The potential energies was determined by calculating the variation in the total energy of the molecule with change in dihedral angle τ (C3C2C8N9 and C4C5C6N7) at intervals of 10° by DFT/6–31G(d,p) method. Two conformer I and II were obtained on potential surface scan. The enolic conformer III was obtained by moving N–H proton to oxygen atom. The enolic conformer III, generally predominates during metal complex formation. The lower energy conformer corresponds to the most stable conformer I. The enthalpy difference between conformer I and II is 0.855 kcal/mol. In principle, the existence of stable compounds would correspond to lower energy conformer. All three conformers are shown in [Fig. 1](#) and molecular graph of lower energy conformer I is shown in [Fig. 2](#). The symmetry observed in N1–C2 and N1–C5 bonds occur due to identical substituents at 2- and 5-positions of pyrrole ring in PDBO. As a result of symmetry in N1–C2 and N1–C5 bonds, delocalization of electron is seen in pyrrole ring and toward azome-

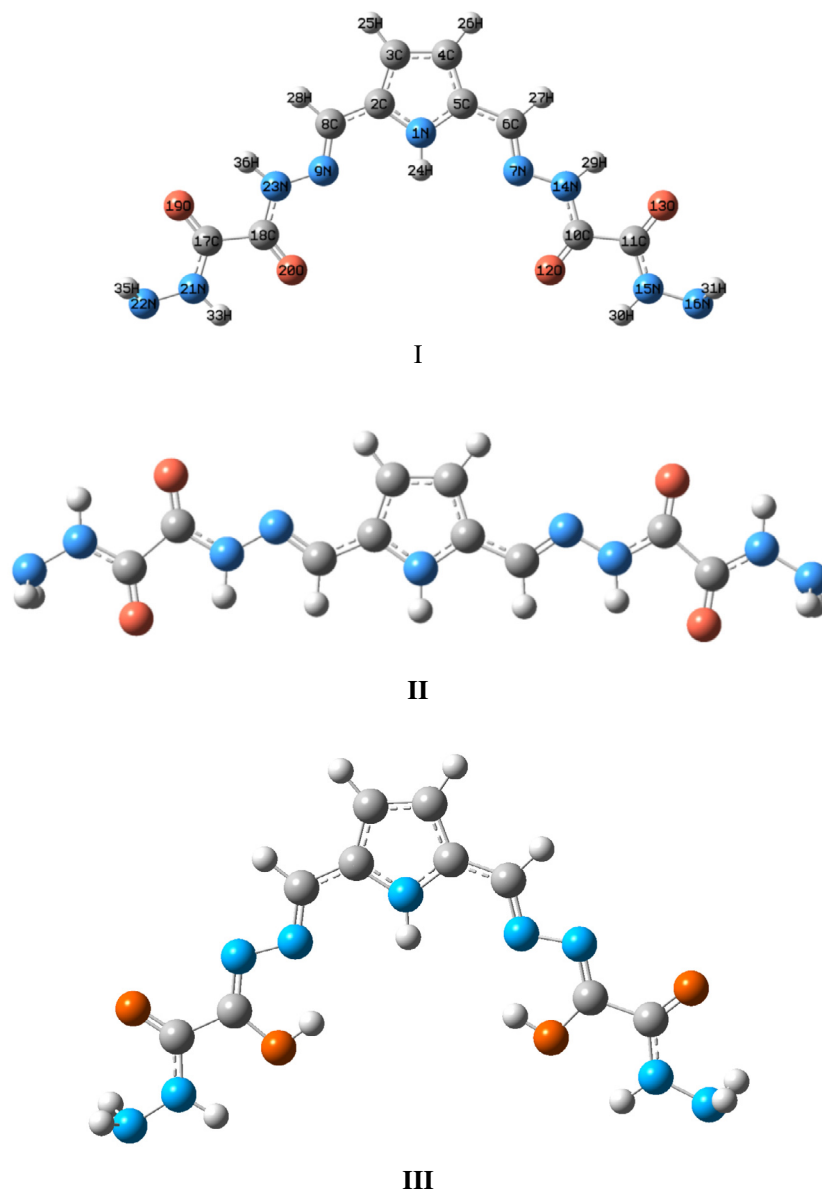


Fig. 1. Optimized geometries for conformers of PDBO.

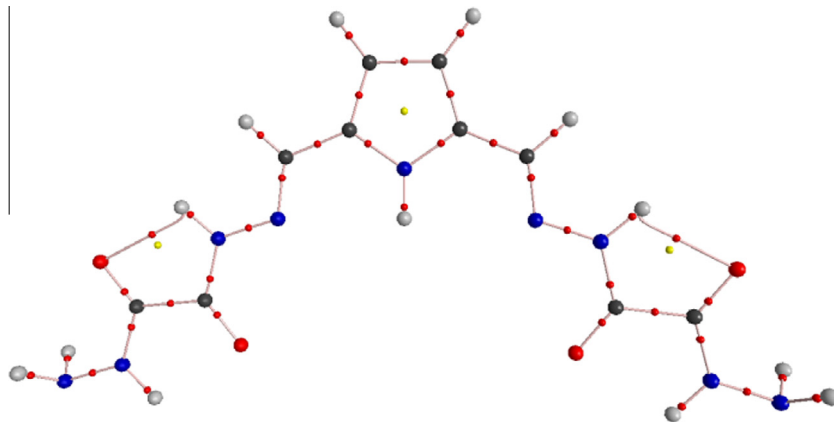


Fig. 2. Molecular graph of PDBO.

thine carbon of PDBO. These effects are observed in quantum calculation and single crystal structure of pyrrole derivatives [33–34]. The presence of C=N, make PDBO to show *E* and *Z* stereoisomers. The *E*-configuration is more stable than *Z*. Considering the thermodynamic stability; *E* isomer is predominant in the mixture. The C=N–NH–(C(=O))₂–NHNH₂ frame is planar and has intramolecular hydrogen bonding between oxygen of carbonyl group and hydrogen of >C=NNH azomethine frame. Popov et al. [24] have reported the crystal structure of pyrrole diisoniazid hydrazone showing the *E* configuration. The calculated optimized bond lengths and bond angles of PDBO using DFT(B3LYP) methods at 6-31G(d,p) and 6-311+G(d,p) basis set are given in Supplementary Tables S1 and Table S2. The bond length calculated by DFT at 6-311+G(d,p) method are more closer with experimental values [17]. Molecular graph of PDBO using AIM program is shown in Fig. 1 and calculated topological parameters is given in Supplementary Table S3. Topological parameters for bonds of interacting atom is calculated at B3LYP/6-31G(d,p) method. The N–H···O interaction visualized in molecular graph is classified as weak intramolecular hydrogen bond due to $(\nabla^2\rho_{BCP}) > 0$ and $H_{BCP} > 0$. According to AIM calculations, the classical intramolecular hydrogen bond (N–H···O) energy is calculated as 5.1 kcal mol⁻¹.

Vibrational assignments

FT-IR spectroscopy is not only frequently used in the literature for the identification of functional group but also used for identification of weaker interaction present in the molecule. In the present study experimental and theoretical data have been compared and presences of weaker interactions have been identified. The experimental and theoretical (selected) vibrational wavenumbers of PDBO and their assignments using PED are given in Table 1. Calculated and experimental IR spectra in the region 4000–400 cm⁻¹ are shown in Fig. 3. The calculated wavenumbers at B3LYP/6-31G(d,p) level are scaled down using single scaling factor 0.9608 to discard the anharmonicity present in real system [35]. The value of correlation coefficient ($r^2 = 0.99$) shows that there is good agreement between experimental and calculated wavenumbers.

N–H Vibrations: In solid state experimental FT-IR spectrum, the N–H stretching vibration of pyrrole (ν_{N-H}) is observed at 3490 cm⁻¹ and calculated as 3502 cm⁻¹ in PDBO. The reported wavenumber of N–H stretching vibration at 3358 cm⁻¹ indicates the involvement of N–H group in weaker bonding as seen in the crystals of pyrrole-2-carbaldehyde isonicotinoyl hydrazone in KBr pellet [36]. The absence of N–H wagging mode at 772 cm⁻¹ confirms free N–H group of pyrrole. The N–H stretch of hydrazide (CONHNH₂) part of molecule is observed at 3480 cm⁻¹, whereas

it is calculated at 3482 cm⁻¹ [37]. In the experimental FT-IR spectrum, asymmetric and symmetric NH₂ stretching vibrations are observed at 3382, 3320 cm⁻¹, with very low intensity corresponds to theoretically calculated wavenumber at 3389, 3319 cm⁻¹, respectively. A combined theoretical and experimental symmetric (3319, 3320 cm⁻¹) and asymmetric (3389, 3382 cm⁻¹) stretching wave number analysis confirms free NH₂ groups in the solid phase of PDBO. The weak band of NH₂ scissoring is assigned at 1580 cm⁻¹, corroborate well with the observed mode at 1639 cm⁻¹ in FT-IR spectrum. The observed NH₂ wagging mode at 855 cm⁻¹ agrees well with the calculated wavenumber at 894 cm⁻¹. The observed NH₂ rocking mode at 1298 cm⁻¹ agrees well with the calculated wavenumber at 1300 cm⁻¹. The vibrational analysis indicates the formation of intramolecular hydrogen bonding (N–H···O). A combined theoretical and experimental symmetric (3386 cm⁻¹) and asymmetric (3458 cm⁻¹) stretching wave number analysis confirms free NH₂ groups in the solid phase of PDBO. The absence of symmetric and asymmetric stretching vibrations in (6) confirms the cyclic product formation that is macrocyclic bis-pyrrole hydrazone.

C–O Vibrations: The observed stretching vibration of carbonyl group ($\nu_{C=O}$) absorption band at 1645 cm⁻¹ agrees well with the calculated wavenumber at 1703 cm⁻¹ which also closely correlates with reported hydrogen bonded $\nu_{C=O}$ vibration at 1665 cm⁻¹ for pyrrole-2-carbaldehyde isonicotinoyl hydrazone [36]. This stretching vibrational wavenumber of carbonyl group again confirms the formation of hydrogen bond (N–H···O) by the involvement of C=O group through intramolecular attraction.

C–N Vibrations: The observed C=N stretching vibration ($\nu_{C=N}$) at 1540 cm⁻¹ agrees well with the calculated wavenumber at 1615 cm⁻¹. In FT-IR spectrum, the presence of C=N band confirms the formation of hydrazone linkage in PDBO and macrocyclic bis-pyrrole hydrazone. The C–N stretches is assigned at 1237 cm⁻¹.

¹H NMR spectroscopy

Pyrrole-2,5-dicarboxaldehyde bis(oxaloyldihydrazone) (5 = PDBO) and macrocyclic bis-hydrazone (6) product were obtained depending on the amount of stoichiometric ratio, solvent and reaction conditions. The experimental and calculated ¹H and ¹³C NMR chemical shifts (δ in ppm) of PDBO are given in Table 2 and experimental spectrum is shown in Supplementary Figs. S1 and S2, respectively. The chemical shifts have been calculated by using DFT (B3LYP) methods with 6-31G(d,p) and 6-311+G(d,p) basis set, employing GIAO approach. The experimental ¹H NMR spectrum of PDBO shows the presence of singlet at δ 4.16 ppm for two free NH₂ protons. The calculated NH signal at δ 9.766 ppm cor-

Table 1
Experimental and calculated vibrational wavenumbers of PDBO at B3LYP/6–31G(d,p) level and their assignments: Wavenumbers ($\bar{\nu}/\text{cm}^{-1}$), Intensity (km mol^{-1}).

$\bar{\nu}$ Unsc	$\bar{\nu}$ Scal	Intensity	$\bar{\nu}$ Obs	Assignment (PED \geq 5%)
3645	3502	62.19	3490	$\nu(\text{N1H24})(99)$
3624	3482	113.96	3480	$\nu(\text{N15H30})(69) \nu(\text{N21H23})(30)$
3528	3389	1.46	3382	$\nu_{\text{as}}(\text{NH}_2)(90)$
3477	3341	9.59		$\nu(\text{N14H29})(53) \nu(\text{N23H36})(46)$
3477	3341	87.26		$\nu(\text{N23H36})(53) - \nu_{\text{as}}(\text{N14H29})(46)$
3454	3319	0.97	3320	$\nu(\text{NH}_2)(80)$
3268	3140	2.7		$\nu(\text{pyCH})(49) \nu(\text{pyCH})(49)$
3254	3126	5.21	3015	$\nu(\text{pyCH})(50) - \nu_{\text{as}}(\text{pyCH})(50)$
3076	2956	14.61	2970	$\nu(\text{C8H28})(41) \nu(\text{C6H27})(36) - \delta_{\text{as}}(\text{C2C9})(18)$
3076	2955	84.11		$\nu(\text{C8H28})(45) - \nu(\text{C6H27})(31) - \delta_{\text{as}}(\text{C2C9})(20)$
1808	1737	410.09	1690	$\nu(\text{C=O})(36) \nu(\text{C18N23})(36) - \nu(\text{C18N23})(6) - \nu(\text{C10N14})(6)$
1800	1729	134.09	1650	$\nu(\text{C18N23})(34) - \nu(\text{C=O})(34) - \nu(\text{C10N14})(5) \nu(\text{C18N23})(5)$
1773	1703	635.08	1645	$\nu(\text{C=O})(71) - \nu(\text{C17N21})(7) - \nu(\text{C11N15})(7)$
1706	1639	100.16	1580	$\delta_{\text{sc}}(\text{NH}_2)(51) \delta_{\text{sc}}(\text{NH}_2)(39)$
1681	1615	139.08	1540	$\delta(\text{N23N9C8})(25) - \nu(\text{C=N})(16) \delta_{\text{as}}(\text{C2C9})(\text{C2C9})(16) \nu(\text{C=N})(14) - \nu(\text{C5C6})(6)$
1668	1603	36.29	1532	$\delta(\text{N23N9C8})(27) - \nu(\text{C=N})(18) \delta_{\text{as}}(\text{C2C9})(17) - \nu(\text{C=N})(16)$
1604	1541	97.23		$\nu(\text{C6H27})(12) - \nu(\text{C2C3})(12) \nu(\text{C=N})(11) - \nu(\text{C=N})(10) - \delta(\text{C5H24N1})(8) \delta(\text{C10H29N14})(5) \delta(\text{N9H36N23})(5)$
1591	1528	164.34	1479	$\delta(\text{N9H36N23})(13) - \delta(\text{C10H29N14})(13) \delta_{\text{as}}(\text{C2C9})(9) \nu(\text{C18N23})(5) \nu(\text{C10N14})(5)$
1567	1506	102.19	1420	$\delta(\text{C10H29N14})(13) \delta(\text{N9H36N23})(13) 78(6) - \nu(\text{C10N14})(6) \nu(\text{C18N23})(6) - \delta(\text{C18C17O20})(5) \delta(\text{C18N23O20})(5)$
1546	1485	248.54	1410	$\rho(\text{NH})(15) - \rho(\text{NH}_2)(15) \delta(\text{NH}_2)(9) - \nu(\text{C11N15})(9) - \nu(\text{C17N21})(9)$
1538	1478	623.62		$\rho(\text{NH})(16) \rho(\text{NH}_2)(16) - \nu(\text{C17N21})(9) \nu(\text{C11N15})(9)$
1521	1462	160.72		$\nu(\text{C3C4})(8) + \nu(\text{C5C6})(8) + \nu(\text{C2C8})(8) + \delta(\text{C10H29N14})(7) - \delta(\text{N9H36N23})(7)$
1466	1409	144.62	1390	$\nu(\text{N1C5})(22) + \nu(\text{N1C2})(22) - \delta(\text{Pyring})(11) - \delta(\text{C5H24N1})(10) - \nu(\text{C2C8})(9) \nu(\text{C2C3})(9)$
1461	1404	30.74		$\nu(\text{C2C3})(13) \nu(\text{C2C8})(13) - \delta(\text{N23N9C8})(11) - \nu(\text{N1C2})(10) - \nu(\text{N1C5})(10)$
1378	1324	31.81	1355	$\nu(\text{C3C4})(25) - \delta_{\text{as}}(\text{C2C9})(22) - \delta(\text{N23N9C8})(10)$
1353	1300	1.13	1298	$\rho(\text{NH}_2)(99)$
1331	1279	52.23	1279	$\delta_{\text{as}}(\text{C2C9})(46) \delta(\text{N23N9C8})(37) \delta(\text{C5C6N7})(8)$
1287	1237	8.26		$\rho(\text{NH}_2)(16) - \delta(\text{O13C11N15})(13) \delta(\text{O13C11C10})(10) - \nu(\text{C6-N7})(9) - \rho(\text{NH})(7) \delta(\text{C=O})(6)$
1287	1237	33.28	1230	$\rho(\text{NH})(16) - \delta(\text{C=O})(14) \rho(\text{C=O})(11) \nu(\text{C17N21})(8) \rho(\text{NH}_2)(7) - \delta(\text{O13C11N15})(5)$
1275	1225	97.98	1205	$\delta(\text{C5H24N1})(33) - \delta(\text{C=N})(11) - \delta(\text{Pyring})(9) - \delta(\text{Pyring})(9) \delta_{\text{as}}(\text{C2C9})(8) \omega(\text{C5H27N7C6})(6)$
1240	1192	146.27	1168	$\delta(\text{C18N23O20})(11) \delta(\text{O12C10C11})(10) - 79(9) \nu(\text{C18N23})(8) - \delta(\text{C18C17O20})(7) - \nu(\text{C10N14})(7) - \delta(\text{N9H36N23})(7) - \delta(\text{C10H29N14})(6)$
1240	1192	54.51	1135	$\delta(\text{O12C10C11})(12) - \rho(\text{C10N14O12})(12) - \delta(\text{C18N23O20})(11) - \nu(\text{C10N14})(8) \delta(\text{C18C17O20})(7) - \nu(\text{C18N23})(7) - \delta(\text{C10H29N14})(7) \delta(\text{N9H36N23})(6)$
1226	1178	76.02		$\delta(\text{N23N9C8})(25) \delta_{\text{as}}(\text{C2C9})(24) - \delta(\text{Pyring})(7) - \delta(\text{Pyring})(7) \nu(\text{C5C6})(6)$
1191	1144	36.08		$\nu(\text{N9N23})(15) \nu(\text{N7N14})(15) \nu(\text{N21N22})(6) \nu(\text{N15N16})(6) \delta(\text{N23N9C8})(5) \delta_{\text{as}}(\text{C2C9})(5)$
1182	1136	57.75		$\nu(\text{N7N14})(13) - \nu(\text{N9N23})(13) \nu(\text{N15N16})(5) - \nu(\text{N21N22})(5) - \nu(\text{C10N14})(5) \nu(\text{C18N23})(5)$
1112	1068	33.34		$\nu(\text{N7N14})(19) - \nu(\text{N9N23})(17) \delta(\text{N14N7C6})(8) - \delta(\text{N23N9C8})(7) \delta(\text{C=N})(5)$
1112	1068	42.1		$\nu(\text{N9N23})(18) \nu(\text{N7N14})(16) \delta(\text{N23N9C8})(7) - \nu(\text{C17N21})(5)$
1073	1031	47.55	1012	$\delta(\text{Pyring})(32) - \delta_{\text{as}}(\text{C2C9})(\text{Pyring})(32)$
1042	1001	0.06		$\delta(\text{Pyring})(16) - \nu(\text{Pyring})(6) - \nu_{\text{as}}(\text{Pyring})(6) - \delta(\text{O12C10C11})(5)$
1037	996	0.27		$\nu(\text{Pyring})(9) - \nu(\text{Pyring})(9) \delta(\text{C5H24N1})(8) \delta(\text{O12C10C11})(5)$
1010	970	54.33	986	$\delta(\text{Pyring})(13) - \omega(\text{NH}_2)(6) - \omega(\text{NH}_2)(6) - \nu(\text{N21N22})(5) - \nu(\text{N15N16})(5) \delta(\text{C=O})(5)$
1008	968	22.5		$\delta(\text{Pyring})(9) \omega(\text{NH}_2)(5) - \omega(\text{NH}_2)(5) \nu(\text{N15N16})(5) - \nu(\text{N21N22})(5)$
957	919	25.76		$\omega(\text{C8H28C2N9})(35) - \omega(\text{H27C6C5N7})(34) - \tau(\text{C6N7})(12) \tau(\text{C8N9})(12)$
955	917	0		$\omega(\text{C8H28C2N9})(33) \omega(\text{H27C6C5N7})(33) - \tau(\text{C8N9})(11) - \tau(\text{C6N7})(11)$
931	894	128.17	855	$\omega(\text{NH}_2)(19) \omega(\text{NH}_2)(17) \nu(\text{N21N22})(14) \nu(\text{N15N16})(13) \delta(\text{C18C17O20})(6) \delta(\text{O12C10C11})(6)$
931	894	161.98	843	$\omega(\text{NH}_2)(20) - \omega(\text{NH}_2)(17) \nu(\text{N15N16})(14) - \nu(\text{N21N22})(13) \delta(\text{O12C10C11})(7) - \delta(\text{C18C17O20})(6)$
851	817	34.46		$\delta(\text{O13C11C10})(16) - \delta(\text{C=O})(16) - \delta(\text{O12C10C11})(10) \delta(\text{C18C17O20})(10) - \delta(\text{O13C11N15})(8) - \delta(\text{C18N23O20})(7) \delta(\text{Pyring})(6)$
849	816	20.66		$\delta(\text{O13C11C10})(17) \delta(\text{C=O})(16) - \delta(\text{O12C10C11})(11) - \delta(\text{C18C17O20})(11) - \delta(\text{O13C11N15})(8) \delta(\text{C18N23O20})(8) \rho(\text{C10N14O12})(5)$
815	783	34.04		$\delta(\text{Pyring})(20) \delta_{\text{as}}(\text{C2C9})(19) - \delta(\text{C=N})(18) \omega(\text{C5H27N7C6})(9) \delta(\text{C18C17O20})(5)$
805	773	1.58		$\delta(\text{N16C11N15})(27) \omega(\text{N21C17C18O19})(24) \omega(\text{C=O})(23) \omega(\text{C10N7N14H29})(21)$
791	760	72.39		$\omega(\text{Pyring})(38) \omega(\text{Pyring})(38)$
766	736	3.2		$\delta(\text{C=N})(23) - \delta_{\text{as}}(\text{C2C9})(17) \omega(\text{C5H27N7C6})(12) - \delta(\text{Pyring})(10) - \delta(\text{N23N9C8})(5)$
701	674	26.68		$\tau(\text{Pyring})(65) - \omega(\text{Pyring})(30)$
678	651	202.45	634	$\tau(\text{N23C18})(20) - \tau(\text{N15C16})(19) - \omega(\text{H29C10N7N14})(18)$
631	606	24.76		$\omega(\text{Pyring})(63) - \tau(\text{Pyring})(20)$
616	592	79.53	558	$\tau(\text{N15C11})(28) - \tau(\text{N21C17})(27) \omega(\text{C=O})(18) \omega(\text{C10N7N14H29})(6)$
549	528	0.41		$\rho(\text{C10N14O12})(17) \delta_{\text{as}}(\text{C2C9})(13) - \delta(\text{C18N23O20})(11) - \delta(\text{C=N})(7) \delta(\text{N23N9C8})(6) - \delta(\text{O12C10C11})(5)$
528	508	2.31		$\rho(\text{C10N14O12})(23) \rho(\text{C=O})(17) \delta(\text{C18N23O20})(14) \delta(\text{O13C11N15})(10) - \delta(\text{O12C10C11})(5)$
512	492	158.97		$\omega(\text{N21C17C18O19})(42) \omega(\text{Pyring})(30) - \tau(\text{Pyring})(20)$
498	479	2.82		$\delta_{\text{as}}(\text{C2C9})(28) - \delta(\text{C=N})(14) - \omega(\text{C5H27N7C6})(8) \delta(\text{C5C6N7})(5)$
419	403	2.81		$\delta(\text{C18C17O20})(18) - \delta(\text{O12C10C11})(15) \delta(\text{N14N7C6})(10) - \delta(\text{C18N23O20})(7) - 49(6) 43(6) 17(5)$

Proposed assignment and potential energy distribution (PED) for vibrational modes: Types of vibrations: ν – stretching, δ_{sc} – scissoring, ρ – rocking, ω – wagging, δ – deformation, δ_s – symmetric deformation, δ_{as} – asymmetric deformation, τ – torsion.

responds to hydrazone (C=NNH) linkage at δ 11.980 ppm in experimental spectrum. Again appearance of singlet at δ 11.895 ppm in experimental spectrum corresponding to calculated signal at δ 8.003 ppm of pyrrolic NHNH_2 proton. The signal appears as singlet at δ 12.191 ppm in experimental spectrum corresponding to calculated signal at δ 9.810 ppm of pyrrolic NH. Appearance of triplet at

δ 6.47–6.69 confirms two vacant β position of pyrrole ring. Sharp singlet at δ 8.771 ppm corresponds to protons of azomethine group directly attached to carbon of hydrazone ($-\text{CH}=\text{NNH}-$) linkage. The disappearance of NH_2 peak in ^1H NMR of macrocyclic bis-hydrazone (6) indicates that (6) exist in cyclic form as shown in [Supplementary Fig. S3](#).

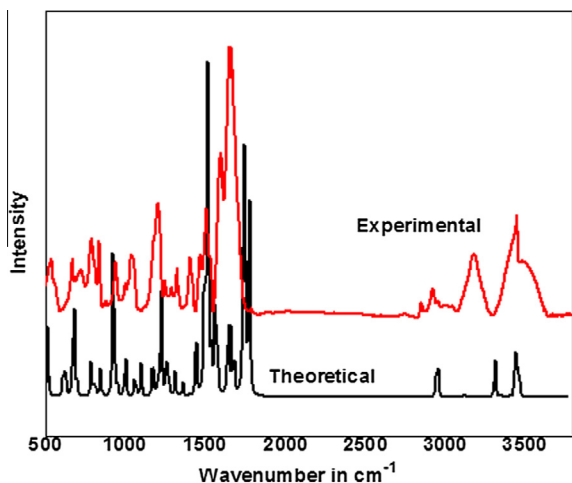


Fig. 3. Comparison between experimental and theoretical IR spectrum for PDBO.

Additional support for the structure of the synthesized compound was provided by its ^{13}C NMR spectrum. The chemical shift values of the carbon atom attached to nitrogen found to be at 138.03 ppm ($\text{C}(\text{H})=\text{N}$) corroborated well with reported hydrazone compound [38]. The values of correlation coefficient for ^1H and ^{13}C NMR ($r^2 = 0.99, 0.99$) show that there are good agreement between experimental and calculated results. In addition to ^1H , ^{13}C NMR chemical shifts, Mass spectrum is shown in Supplementary Figs. S4 and S5 also confirms the presence of molecular ion peak at $M+1$, corresponds to the molecular formula $\text{C}_{10}\text{H}_{13}\text{N}_9\text{O}_4$ and $\text{C}_{16}\text{H}_{14}\text{N}_{10}\text{O}_4$ of PDBO and macrocyclic bis-hydrazone (6), respectively.

Natural bond orbital analysis and UV–visible spectrum

The NBOs provides an accurate method for studying intra-, inter-molecular bonding, interaction among bonds and charge transfer or conjugative interaction in various molecular systems [39]. The second-order perturbation theory analysis of Fock Matrix, in the NBO basis for PDBO, calculated at B3LYP/6-31G(d,p) are presented in Table 3. The delocalization of π electron from $\pi(\text{C}2-\text{C}3) \rightarrow \sigma^*(\text{C}2-\text{C}8)/\sigma^*(\text{N}1-\text{C}2)/\pi^*(\text{C}4-\text{C}5)/\pi^*(\text{C}8-\text{N}9)$ stabilized the molecule up to 21.46 kcal mol $^{-1}$ due to strong conjugative interactions. The another conjugative interactions $n_2(\text{O}20) \rightarrow \sigma^*(\text{C}17-\text{C}18)/\pi^*(\text{C}18-\text{N}23)$, $n_1(\text{O}13) \rightarrow \sigma^*(\text{C}11-\text{N}15)/\sigma^*(\text{C}10-\text{C}11)$ and $n_1(\text{O}19) \rightarrow \sigma^*(\text{C}11-\text{C}18)/\sigma^*(\text{C}17-\text{C}21)$ stabilized the molecule up to 24.39 kcal mol $^{-1}$. The structure allow strong $\pi-\pi^*$ and $n-\pi^*$ transitions in the UV–visible region with high extinction coefficients.

Table 2

Calculated and experimental ^1H NMR and ^{13}C NMR chemical shifts (δ/ppm) in chemical shifts (δ/ppm) in DMSO of (5 = PDBO).

Atom no.	δ calcd.		δ exp.	Assignment	Atom no.	δ calcd.		δ exp.	Assignment
	6-31G(d,p)	6-311+G(d,p)				6-31G(d,p)	6-311+G(d,p)		
24H	9.382	9.810	12.19	(s, 1H, pyrrole–NH)	2C	126.06	139.018	123.63	(pyrrole ring)
25H	6.133	6.411	6–48–6.69	(d, 2H, pyrrole–CH)	3C	110.798	121.436	117.99	(pyrrole ring)
26H	6.133	6.411	6–48–6.69	(d, 2H, pyrrole–CH)	4C	110.797	121.4363	117.99	(pyrrole ring)
27H	7.075	7.617	8.77	(s, 1H, –CH=N)	5C	126.061	139.019	129.27	(pyrrole ring)
28H	7.074	7.617	8.77	(s, 1H, –CH=N)	6C	128.482	139.649	138.00	(hydrazone–CH=N–NH)
29H	9.388	9.766	11.98	(s, 1H, hydrazide–C=N–NH)	8C	128.482	139.649	138.00	(hydrazone–CH=N–NH)
30H	7.699	8.002	11.89	(s, 1H, hydrazide–NH–NH ₂)	10C	145.896	157.351	161.57	(amidic–NH–COCONH)
31H	2.786	3.206	4.16	(s, 1H, –NH ₂)	11C	154.834	167.696	157.43	(amidic–NH–COCONH)
32H	2.785	3.205	4.16	(s, 1H, –NH ₂)	17C	154.836	167.6989	157.43	(amidic–NH–COCONH)
33H	7.699	8.002	11.89	(s, 1H, hydrazide–NH–NH ₂)	18C	145.895	157.350	161.57	(amidic–NH–COCONH)
34H	2.787	3.207	4.16	(s, 1H, –NH ₂)					
35H	2.784	3.203	4.16	(s, 1H, –NH ₂)					
36H	9.388	9.766	11.98	(s, 1H, hydrazide–C=N–NH)					

TD-DFT/B3LYP calculation using 6-31G(d,p)/6-311+G(d,p) basis set have been used to determine the low-lying excited states of PDBO. The experimental values and calculated electronic transitions of high oscillatory strength are listed in Table 4. Comparison between experimental and theoretical UV–visible spectrum is shown in Fig. 4. The TD-DFT calculations predict one intense electronic transitions at $\lambda_{\text{max}} = 382$ nm, $f = 0.796$ (B3LYP/6-31 g(d,p)) and $\lambda_{\text{max}} = 397$ nm, $f = 0.7959$ (B3LYP/6-311+g(d,p)). The calculated electronic transitions at $\lambda = 266$ nm (B3LYP/6-31g(d,p)) and 274 nm (B3LYP/6-311+g(d,p)) are correspond to the experimental electronic transitions observed at $\lambda = 287$ nm. According to the TD-DFT calculations, the experimental bands at 287 nm originate mainly due to the electronic excitations $\text{H}-3 \rightarrow \text{L}$. The difference between the theoretical and experimental UV–visible spectra is due to solvation.

Chemical reactivity

The most fruitful and promising framework so far is probably the Density Functional Theory of chemical reactivity so called conceptual DFT [40]. Conceptual DFT is a subfield of DFT in which one tries to extract from the electronic density relevant concepts and principles that help to understand and predict the chemical behavior of a molecule. The calculated global parameters [41,42] are given in Table 5.

According to Mulliken [52] chemical potential and the electronegativity is calculated as

$$\mu = -\chi = -1/2(I + A) \quad (1)$$

$$\eta = 1/2(I - A) \quad (2)$$

where I and A are the first ionization energy and electron affinity, respectively. The chemical potential and the absolute electronegativity are molecular properties and not the orbital properties. According to Koopman's [53] theorem the I is simply the eigenvalue of HOMO with change of sign and A is the eigenvalue of LUMO with change of sign, hence the Eq. (1) can be written as

$$-\chi = -1/2(\varepsilon_{\text{HOMO}} + \varepsilon_{\text{LUMO}}) \quad (3)$$

$$\eta = 1/2(\varepsilon_{\text{LUMO}} - \varepsilon_{\text{HOMO}}) \quad (4)$$

The electrophilicity index, $(\omega) = \mu^2/2\eta$ which measures the capacity of an electrophile to accept the maximal number (a fractional of or more than one) of electrons in a neighboring reservoir of electron sea.

The local reactivity descriptors [40–51] such as Fukui functions $f_k^+(r)$, $f_k^-(r)$ are calculated using the following equations as:

$$f_k^+(r) = [q_k(N+1) - q_k(N)], \text{ for nucleophilic attack} \quad (5)$$

$$f_k^-(r) = [q_k(N) - q_k(N-1)], \text{ for electrophilic attack} \quad (6)$$

Table 3
Second-order perturbation theory analysis of the Fock matrix in NBO basis for monomer: Donor (*i*), Acceptor (*j*), Occupancy (O), Percentage electron density over bonded atoms (ED_x, %), Stabilization energy of charge delocalization interactions($E^{(2)}$) in (kcal/mol) and NBO hybrid orbitals of bonded atoms of (5 = PDBO).

Donor			Acceptor			$E^{(2)}$
(<i>i</i>)/O (<i>i</i>)	ED _A ED _B (%)	NBO hybrid orbitals	(<i>j</i>) / O (<i>j</i>)	ED _A (%) ED _B (%)	NBO hybrid orbitals	
σ (N1–H24) 1.988	74.24	0.8616(sp ^{2.33}) _N +	σ^* (N1–C2)	68.72	0.8290 (sp ^{2.59}) _N –0.5593(sp ^{2.04}) _H	0.68
	25.76	0.5075(sp ⁰) _H	0.08889	31.28		
			σ^* (C4–C5)	51.34	0.7165(sp ^{2.03}) _N –0.6976(sp ^{1.72}) _H	1.99
σ (N15–H30) 1.984	73.26	0.8559(sp ^{2.15}) _N +	0.01546	48.66		
	26.74	0.5171(sp ⁰) _H	σ^* (C11–O13)	64.89	0.8056(sp ^{2.01}) _N –0.5925(sp ^{1.48}) _H	5.09
			0.01316	35.11		
σ (N1–C2) (1.983)	61.68	0.7854 (sp ^{1.86}) _N +	σ^* (N1–C5)	38.32	0.6190(sp ^{1.86}) _N –0.7854(sp ^{2.71}) _H	1.96
	38.32	0.6190 (sp ^{2.71}) _H	0.02340	61.68		
			σ^* (C2–C3)	48.66	0.6976(sp ^{1.72}) _N –0.7165(sp ^{2.03}) _H	1.39
σ (N1–C5) (1.983)	61.68	0.7854 (sp ^{1.86}) _N +	0.01546	51.34		
	38.32	0.6190 (sp ^{2.71}) _H	σ^* (C5–C6)	48.90	0.6993(sp ^{1.76}) _N –0.7148(sp ^{1.82}) _H	3.82
			0.02570	51.10	0.6993(sp ^{1.76}) _N –0.7148(sp ^{1.82}) _H	1.28
π (C2–C3) (1.712)	50.00	0.7071 (sp ^{1.00}) _N +	σ^* (C2–C8)	48.90	0.6993(sp ^{1.76}) _N –0.7148(sp ^{1.82}) _H	3.14
	50.00	0.7071 (sp ^{1.00}) _H	0.02570	51.10		
			σ^* (N1–C2)	38.32	0.6190(sp ^{1.86}) _N –0.7854(sp ^{2.71}) _H	3.43
π (C4–C5) (1.712)	50.00	0.7071 (sp ^{1.00}) _N +	0.02340	61.68		
	50.00	0.7071 (sp ^{1.00}) _H	π^* (C4–C5)	50.00	0.7071(sp ^{1.00}) _N –0.7071(sp ^{1.00}) _H	19.95
			0.41417	50.00		
π (C8–N9) (1.712)	43.24	0.6576 (sp ^{1.00}) _N +	π^* (C8–N9)	56.76	0.7534(sp ^{1.00}) _N –0.6576(sp ^{1.00}) _H	21.46
	56.76	0.7534 (sp ^{1.00}) _H	0.23441	43.24		
			π^* (C2–C3)	50.00	0.7071(sp ^{1.00}) _N –0.7071(sp ^{1.00}) _H	19.95
π (C6–N7) (1.918)	43.24	0.6576 (sp ^{1.00}) _N +	0.41417	50.00		
	56.76	0.7534 (sp ^{1.00}) _H	π^* (C6–N7)	56.76	0.7534(sp ^{1.00}) _N –0.6576(sp ^{1.00}) _H	21.46
			0.23441	43.24		
σ (C3–C4) (1.975)	50.00	0.7071 (sp ^{1.95}) _N +	σ^* (N1–H24)	25.76	0.5075(sp ^{2.33}) _N –0.8616(sp ^{0.00}) _H	3.43
	50.00	0.7071 (sp ^{1.95}) _H	0.01759	74.24		
			σ^* (C5–C6)	48.90	0.6993(sp ^{1.76}) _N –0.7148(sp ^{1.82}) _H	3.41
σ (C2–C8) (1.976)	51.10	0.7148 (sp ^{1.76}) _N +	0.02570	51.10		
	48.90	0.6933 (sp ^{1.82}) _H	σ^* (C5–C6)	48.90	0.6993(sp ^{1.76}) _N –0.7148(sp ^{1.82}) _H	5.74
			0.02570	51.10	0.6993(sp ^{1.76}) _N –0.7148(sp ^{1.82}) _H	5.74
σ (C5–C6) (1.976)	51.10	0.7148 (sp ^{1.76}) _N +	0.02570	51.10		
	48.90	0.6933 (sp ^{1.82}) _H	σ^* (N9–N23)	53.16	0.7291(sp ^{3.06}) _N –0.6844(sp ^{2.82}) _H	4.44
			0.02154	46.84		
π (C8–N9) (1.712)	43.24	0.6576 (sp ^{1.00}) _N +	σ^* (C2–C3)	48.66	0.6976(sp ^{1.72}) _N –0.7165(sp ^{2.03}) _H	3.01
	56.76	0.7534 (sp ^{1.00}) _H	0.01546	51.34		
			σ^* (C2–C3)	48.66	0.6976(sp ^{1.72}) _N –0.7165(sp ^{2.03}) _H	3.01
π (C6–N7) (1.918)	43.24	0.6576 (sp ^{1.00}) _N +	0.01546	51.34		
	56.76	0.7534 (sp ^{1.00}) _H	σ^* (C4–C5)	48.66	0.7165(sp ^{2.03}) _N –0.6976(sp ^{1.72}) _H	10.35
			0.01546	48.66		
σ (C10–N14) (1.988)	37.18	0.6098 (sp ^{2.08}) _N +	σ^* (C6–N7)	59.36	0.7705(sp ^{2.05}) _N –0.6375(sp ^{1.44}) _H	1.98
	62.82	0.7926 (sp ^{1.66}) _H	0.00692	40.64		
			σ^* (C8–N9)	59.36	0.7705(sp ^{2.05}) _N –0.6375(sp ^{1.44}) _H	1.98
σ (C18–N23) (1.988)	37.18	0.6098 (sp ^{2.08}) _N +	0.00692	40.64		
	62.82	0.7926 (sp ^{1.66}) _H	σ^* (C18–N23)	62.82	0.7926(sp ^{2.08}) _N –0.6098(sp ^{1.66}) _H	1.25
			0.07745	37.18		
σ (C17–N21) (1.982)	38.23	0.6183 (sp ^{2.08}) _N +	σ^* (C10–N14)	62.82	0.7926(sp ^{2.08}) _N –0.6098(sp ^{1.66}) _H	1.25
	61.77	0.7860 (sp ^{1.66}) _H	0.07745	37.18		
			σ^* (C10–N14)	62.82	0.7926(sp ^{2.08}) _N –0.6098(sp ^{1.66}) _H	1.25
σ (N15–C11) (1.982)	38.23	0.6183 (sp ^{2.08}) _N +	0.07745	37.18		
	61.77	0.7860 (sp ^{1.66}) _H	π^* (C10–C11)	48.29	0.6949(sp ^{1.85}) _N –0.7191 (sp ^{1.53}) _H	2.64
			0.05521	51.71		
n_2 O12 1.852		sp ^{99.99}	σ^* (C17–C18)	49.72	0.7051(sp ^{1.95}) _N –0.7091(sp ^{1.99}) _H	22.89
			0.12286	50.28		
			π^* (C18–N23)	62.82	0.7926(sp ^{2.08}) _N –0.6098(sp ^{1.66}) _H	27.32
n_2 O20 1.852		sp ^{99.99}	0.08889	37.18		

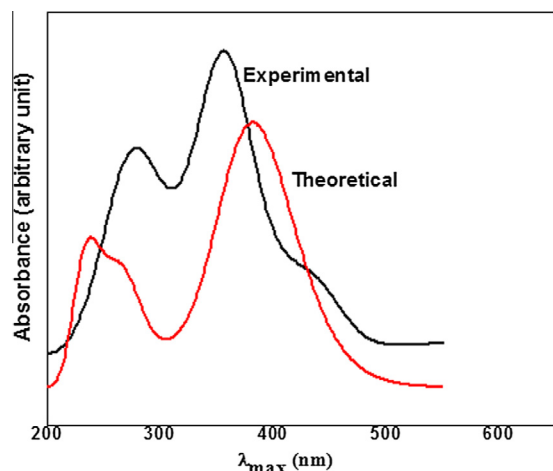
Table 3 (continued)

Donor			Acceptor			$E^{(2)}$
(i)/O (i)	ED _A ED _B (%)	NBO hybrid orbitals	(j) / O (j)	ED _A (%) ED _B (%)	NBO hybrid orbitals	
n_2O13 1.860		sp ^{99.99}	$\sigma^*(C11-N15)$ 0.35496	72.85 27.15	0.8535 (sp ¹) _N -0.5210 (sp ¹) _H	24.39
			$\sigma^*(C10-C11)$ 0.12285	50.28 49.72	0.7091(sp ^{1.99}) _N -0.7051(sp ^{1.95}) _H	21.54
n_2O19 1.860		sp ^{99.99}	$\sigma^*(C11-C18)$ 0.03449	49.72 50.28	0.7051(sp ^{1.95}) _N -0.7091(sp ^{1.99}) _H	21.25
			$\sigma^*(C17-C21)$ 0.07719	61.77 38.23	0.7860(sp ^{2.03}) _N -0.6183(sp ^{1.57}) _H	24.39

Table 4

Calculated and experimental electronic excitations for (5 = PDBO).

6-31G(d,p)		6-311+G(d,p)			
Excitations	λ calcd.	Excitations	λ calcd	λ obs.	Assignment
84 → 85 (H → L)	382.98	84→85	397.45	381	$\pi \rightarrow \pi^*$
84 → 86 (H → L+1)	322.15	84→86	329.83		
81 → 85(H-3 → L)	266.40	81→85	274.18	287	
78 → 85 (H-7 → L)	248.78	78→85	242.83		$\pi \rightarrow \pi^*$

**Fig. 4.** Comparison between experimental and theoretical UV-visible spectra for PDBO.

where, q is the gross charge of atom k in the molecule and N , $N+1$, $N-1$ are electron systems containing neutral, anion, cation form of molecule, respectively. Using Fukui functions, other local reactivity descriptors as local softnesses (s_k^+ , s_k^-) and electrophilicity indices (ω_k^+ , ω_k^-) are calculated using following equations as

$$s_k^+ = S f_k^+, s_k^- = S f_k^- \quad (7)$$

$$\omega_k^+ = \omega f_k^+, \omega_k^- = \omega f_k^- \quad (8)$$

where, + and - sign show nucleophilic, electrophilic attack, respectively.

The orbitals play a major role in governing many chemical reactions, and are also responsible for charge transfer complexes. The

Table 5

Calculated ϵ_{HOMO} , ϵ_{LUMO} , energy band gap ($\epsilon_L - \epsilon_H$), chemical potential (μ), electronegativity (χ), global hardness (η), global softness (S) and global electrophilicity index (ω) for (1), (2), and (5 = PDBO), Electrophilicity based charge transfer (ECT) for reactant system [(1) ↔ (2)].

	ϵ_H	ϵ_L	$(\epsilon_L - \epsilon_H)$	χ	μ	η	S	ω	ECT
(1)	-6.8410	-2.3647	4.4763	4.6028	-4.6028	2.2382	0.2234	4.7330	0.6496
(2)	-6.7803	-1.1461	5.6341	3.9632	-3.9632	2.8170	0.1774	2.7878	
(3)	-5.5493	-2.1388	3.4104	3.8440	-3.8440	1.7052	0.2932	4.3328	

ϵ_H , ϵ_L , ($\epsilon_H - \epsilon_L$), χ , μ , η , ω (in eV) and S (in eV⁻¹).

treatment of the frontier molecular orbitals separately from the other orbitals is based on the general principles governing the nature of chemical reactions. The energy of the HOMO is directly related to the ionization potential and characterizes the susceptibility of the molecule toward attack of electrophiles. The energy of LUMO is directly related to the electron affinity and characterizes the susceptibility of the molecule toward attack of nucleophiles. The concept of hard and soft nucleophiles and electrophiles has been also directly related to the relative energies of the HOMO and LUMO orbitals.

Electrophilic charge transfer [54] (ECT) = (ΔN_{max})_A - (ΔN_{max})_B is defined as the difference between the ΔN_{max} values of interacting molecules. If we consider two molecules **1** and **2** approach to each other (i) if ECT > 0, charge flow from **2** to **1** (ii) if ECT < 0, charge flow from **1** to **2**. The calculated high value of electrophilicity index shows that reactant **1** is a strong electrophile than reactant **2**. The Electrophilic charge transfer ECT is calculated as 0.6496 for reactant molecules **1** and **2**, which indicates that charge flows from **2** to **1**. Selected electrophilic reactivity descriptors (f_k^+ , s_k^+ , ω_k^+) for reactant **1** and nucleophilic reactivity descriptors (f_k^+ , s_k^- , ω_k^-) for reactant **2**, using Hirshfeld population analyses are listed in Table 6. In reactant **1**, the maximum values of the local electrophilic reactivity descriptors (f_k^+ , s_k^+ , ω_k^+) at C (6/7) indicate that this site is prone to nucleophilic attack. In the same way, for reactant **2**, the maximum values of the local nucleophilic reactivity descriptors (f_k^+ , s_k^- , ω_k^-) at N (6) indicate that this is more nucleophilic site. Therefore, local reactivity descriptors for reactants **1** and **2** confirm the formation of product by nucleophilic attack of N (6) site of reactant **2** on the more electrophilic C (6/7) site of reactant **1**.

Selected reactivity descriptors as Fukui functions (f_k^+ , f_k^-), local softnesses (s_k^+ , s_k^-), local electrophilicity indices (ω_k^+ , ω_k^-) for (5 = PDBO), using Hirshfeld atomic charges are given in Table 7. In PDBO, the maximum values of the electrophilic reactivity

Table 6

Selected electrophilic reactivity descriptors (f_k^+ , s_k^+ , ω_k^+) for reactant (1) and nucleophilic reactivity descriptors (f_k^- , s_k^- , ω_k^-) for reactant (2) using Hirshfeld population analyses charges.

Reactant (1)				Reactant (2)			
Sites	f_k^+	s_k^+	ω_k^+	Sites	f_k^-	s_k^-	ω_k^-
C6	0.1053	0.0235	0.4989	N5	0.056658	0.010056	0.157954
C7	0.1053	0.0235	0.4989	N6	0.119492	0.021207	0.333126
				N7	0.066731	0.011843	0.186036
				N8	0.131873	0.023405	0.367642

f_k^+ , f_k^- (in e); s_k^+ , s_k^- (in eV^{-1}) and ω_k^+ , ω_k^- (in eV).

descriptors (f_k^+ , s_k^+ , ω_k^+) at C6/C8 indicate that this site is more prone to nucleophilic attack. Therefore, local reactivity descriptors of PDBO favor the formation of new heterocyclic compounds such as thiadiazoline, thiazolidinones and azetidinones etc. by attack of nucleophilic part of the dipolar reagent on the C6/C8 site of C8=N9/C6=N7 bond. In the same way, for PDBO the maximum values of the nucleophilic reactivity descriptors (f_k^- , s_k^- , ω_k^-) at nitrogen atom of N16/N22 indicate that this site is more prone to electrophilic attack and favor the formation of Schiff base and hydrazide-hydrazones compounds.

Atomic charges

The charge distribution of PDBO was calculated from the atomic charges by NBO and Mulliken population analysis (Fig. 5). The atomic charges are calculated using B3LYP method with 6-31G(d,p)/6-311+G(d,p) basis set and the values are tabulated in Supplementary Table S4. The charges changes with basis set presumably occur due to polarization. These two basis set does not predict the same trend i.e., among the nitrogen atoms N1 and N16/22, N16/22 is considered as basic site, opposite trend is observed in case of MPA charges [55]. The charge distribution shows that the more negative charge is concentrated on N16/22 atom of NH₂ group whereas the positive charge resides at hydrogen atoms. Among the oxygen atoms O12/20 and O13/19, O13/19 is considered more electronegative than O12/20. The negative charge concentrated at O12/20 share with hydrogen atom of N14-H29/N23-H36 due to intramolecular hydrogen bonding. All the hydrogen atoms have a net positive charge. Considering both bases sets used in the atomic charge calculation; the oxygen atoms exhibit a negative charge, which are donor atoms. Hydrogen atom exhibits a positive charge, which is an acceptor atom, may suggest the presence of intra-molecular bonding in the gas phase.

Molecular electrostatic potential surface

Molecular electrostatic potential are useful quantities to illustrate the charge distributions of molecules and used to visualize variably charged regions of a molecule. Therefore, the charge distributions can give information about how the molecules interact with another molecule. Molecular electrostatic potential is widely used as a reactivity map displaying most probable regions for the electrophilic attack of charged point-like reagents on organic molecules [56].

ESP provides a visual method to understand the relative polarity of a molecule. It also serves as a useful quantity to explain electronegativity, partial charges, site of chemical reactivity, structure-activity relationship, hydrogen bonding and other interactions of molecules including biomolecules and drugs. Molecular electrostatic potential [$V(r)$] of a molecule is expressed by the following equation [57] given as:

$$V(r) = \sum Z_A/|R_A - r| - \int \rho(r)dr'/|r' - r|$$

Table 7

Selected electrophilic reactivity descriptors (f_k^+ , s_k^+ , ω_k^+) and nucleophilic reactivity descriptors (f_k^- , s_k^- , ω_k^-) for (5 = PDBO) using Hirshfeld population analyses charges.

Sites	f_k^+	s_k^+	ω_k^+	Sites	f_k^-	s_k^-	ω_k^-
C6/C8	0.1492	0.0437	0.6464	N1	0.3368	0.0987	1.4592
O12/	0.0715	0.0209	0.3097	N14/	0.2676	0.0784	1.1594
O20				N23			
O13/	0.0418	0.0122	0.1811	N15/	0.3102	0.0909	1.3440
O19				N21			
				N16/	0.5576	0.1634	2.4159
				N22			

f_k^+ , f_k^- (in e); s_k^+ , s_k^- (in eV^{-1}) and ω_k^+ , ω_k^- (in eV).

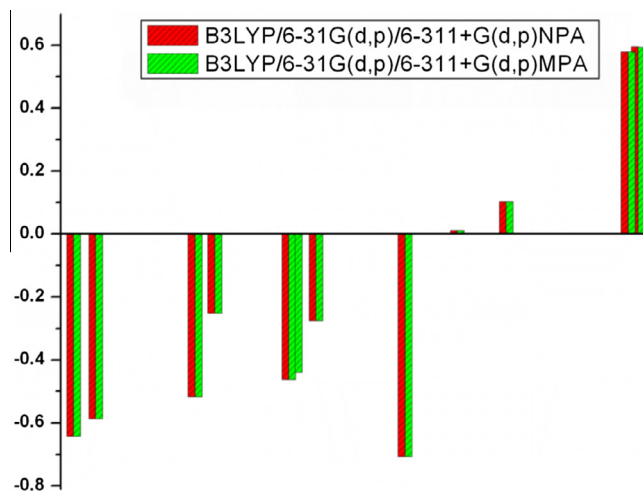


Fig. 5. Bar diagram representing the charge distribution of PDBO using NPA and MPA methods.

where, Z_A is the charge on nucleus A located at R_A and $\rho(r)$ is the electron density. The first term in the expression represents the effect of the nuclei and the second represents that of electrons. The two terms have opposite sign and therefore opposite effects. $V(r)$ is their resultant at each point r and it is an indication of the net electrostatic effect produced at the point r by the total charge distribution (electron+nuclei) of the molecule.

The molecular electrostatic potential is related to electron density and a very useful descriptor for determining sites for electrophilic attack and nucleophilic reactions as well as hydrogen-bonding interactions. To predict reactive sites for electrophilic and nucleophilic attack for the investigated molecule, the MEP at the B3LYP/6-31G(d,p) optimized geometry was calculated and shown in Fig. 6. The different values of the electrostatic potential at the surface are represented by different colors. Potential increases in the order red < orange < yellow < green < blue. The negative (red, orange and yellow) regions of the MEP are related to electrophilic reactivity. The maximum positive region is localized on the NH bonds, indicating a possible site for nucleophilic attack. The MEP map (Fig. 6) shows that the negative potential sites are on electronegative O atom and the positive potential sites are around the hydrogen atoms of azomethine (CH=NNH) frame. These sites give information about the region from where the compound can have intermolecular interactions. This predicted the most reactive site for both electrophilic and nucleophilic attack.

First hyperpolarizability

Experimental measurements and theoretical calculations on molecular hyperpolarizability β is one of the key factors in the

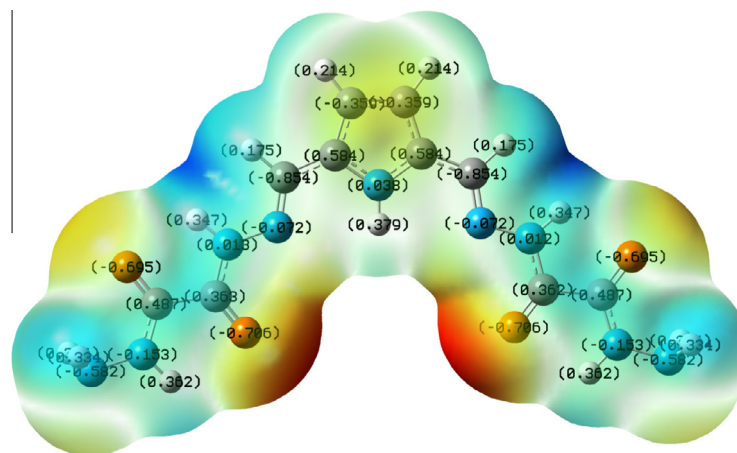


Fig. 6. Molecular electrostatic potential (ESP) map for PDBO.

Table 8

Calculated dipole moment (μ_0), polarizability ($|\alpha_0|$), anisotropy of polarizability ($\Delta\alpha$), First hyperpolarizability (β_0) and their components calculated at B3LYP/6-31G(d,p) of (5 = PDBO).

Dipole moment		Polarizability		Hyperpolarizability	
μ_x	0.0003	α_{xx}	381.699	β_{xxx}	3.4924
μ_y	4.5484	α_{yy}	20.75	β_{xxy}	-2486.11
μ_z	0.1935	α_{zz}	26.302	β_{xyy}	-1.339
μ_0	4.5525	$ \alpha_0 $	21.1803	β_{yyy}	-283.69
		$\Delta\alpha$	111.436	β_{xxz}	-2.545
				β_{xyz}	-2.126
				β_{yyz}	-1.485
				β_{xzz}	0.374
				β_{yzz}	10.730
				β_{zzz}	-1.690
				β_0	23.836
Para nitro aniline (p-NA)					
B3LYP/6-31G(d,p)					
μ_0	7.5769	$ \alpha_0 $	12.798	β_0	11.546
		$\Delta\alpha$	38.396		

μ_0 /Debye; $|\alpha_0|$ and $\Delta\alpha/10^{-24}$ esu; $\beta_0/10^{-30}$ esu.

second order NLO materials design. Theoretical determination of hyperpolarizability is quite useful both in understanding the relationship between the molecular structure and nonlinear optical

properties. Polarizabilities and hyperpolarizabilities are described to response of a system in the presence of an applied electric field [58]. They determine the strength of molecular interactions (long-range intermolecular induction, dispersion forces, etc.), cross sections of different scattering and collision processes, as well as the non-linear optical (NLO) properties of the system. The DFT-based methods can be of great aid and adequate in searching for new nonlinear chemical compounds [59]. Theoretical methods have been considered as useful techniques for prediction of polarizabilities and hyperpolarizabilities avoiding an expensive large amount of experimental synthetic work that precedes the measuring of NLO properties, what may not lead to a desired compound for practical applications [58]. The search for molecules possessing a large value of static first hyperpolarizability is a key step toward the optimization of new materials for NLO response applications. Hybrid functional, B3LYP, tend to be the most commonly used methods for computational chemistry practitioners [60]. In order to investigate the relationship between molecular structure and NLO response, first hyperpolarizability (β_0) of this novel molecular system, and related properties ($|\alpha_0|$ and $\Delta\alpha$) are calculated using B3LYP/6-31G(d,p), based on the finite-field approach and their calculated values are given in Table 8. It is well known that if the molecule has many delocalization π electrons, bigger change of dipole moment from ground state to excited state, large transition

Table 9

The antimicrobial activity of reactants (r1, r2) and product (P = PDBO)) at different concentration.

Comp	Antibacterial activity							
	Zone of inhibition(mm)							
	Gram positive				Gram negative			
	<i>S. aureus</i>		<i>S. pyogenes</i>		<i>E. coli</i>		<i>P. aeruginosa</i>	
	$\mu\text{g/ml}$	$\mu\text{g/ml}$	$\mu\text{g/ml}$	$\mu\text{g/ml}$	$\mu\text{g/ml}$	$\mu\text{g/ml}$	$\mu\text{g/ml}$	$\mu\text{g/ml}$
r1	100	200	100	200	100	200	100	200
r2	6	11	6	10	5	9	4	9
P	9	12	9.3	12	7	13	7	13
Control	11	18	10	17	9	17	8	17
chloramphenicol	14	20	13	20	13	23	13	19
Comp	Antifungal activity							
	<i>C. albicans</i>		<i>A. niger</i>					
	$\mu\text{g/ml}$	$\mu\text{g/ml}$	$\mu\text{g/ml}$	$\mu\text{g/ml}$				
	r1	100	200	100	200			
	r2	6	9	8	11			
P	7	11	10	14				
Nystatin	10	17	11	21				
	12.5	22	14	25				

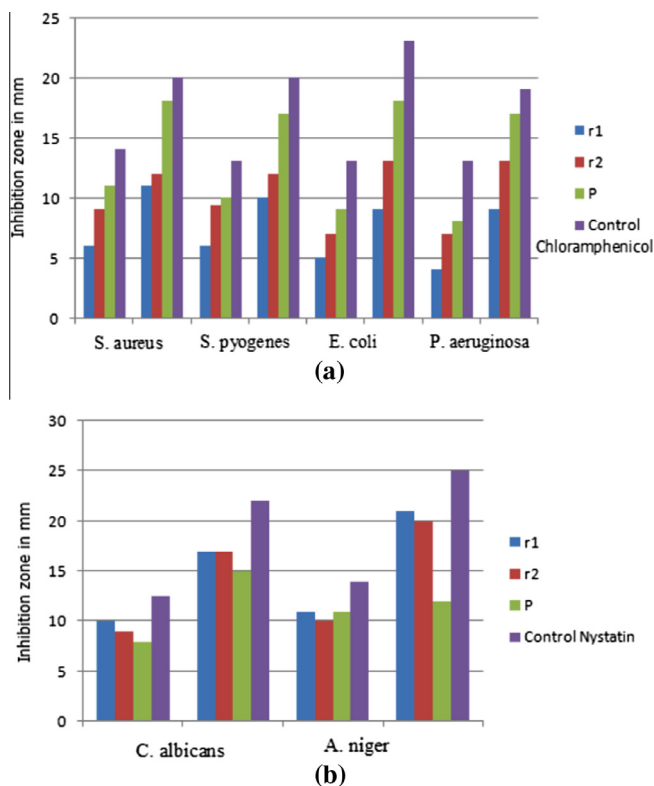


Fig. 7. Bar diagram represent the inhibition zone in mm of (a) against bacterial strains (b) against fungal strains.

moment and noncentrosymmetry structure, the molecule will have strong second order NLO response [61].

In this study, *p*-nitroaniline (*p*-NA) is chosen as a reference molecule because there were no experimental values for PDBO molecule. The *p*-NA is one of the prototypical molecules used in the study of the NLO properties of molecular systems [62]. Para-nitroaniline (PNA) is such a material which known for its nonlinear optical properties. In PNA, the presence of a desirable resonance structure, in addition to the intermolecular charge transfer, leads to high value of polarizability (α) and hyperpolarizability (β). The first hyperpolarizability (β_0) of the title compound is calculated as 23.83×10^{-30} esu which is approximately twice of reference molecule *p*-nitroaniline (*p*-NA, $\beta_0 = 11.54 \times 10^{-30}$ esu). Therefore, investigated molecule is suitable for non-linear optical applications.

Antimicrobial activity

All the compound and reactants reported in Table 9 showed a good antibacterial and antifungal activity. Fig. 7 shows bar diagram for representation of Zone inhibition in mm of (a) against bacterial strains (b) against fungal strains. The product PDBO shows good antibacterial activity in comparison to 2,5-diformyl-1*H*-pyrrole and oxalic acid dihydrazide. The product PDBO was found more active against gram positive *S. aureus* and *S. pyogenes* bacterial strain at $\mu\text{g/ml}$ concentration. The reactant (r1) found in most of the case less active against both gram positive and gram negative bacteria. The results of preliminary antifungal activity screening reveals that PDBO has significant effect on *C. albicans* and *A. niger*, even at 100 $\mu\text{g/ml}$ concentration, though the best results comes only at 200 $\mu\text{g/ml}$ respectively. In all cases the assayed substances showed an activity level against bacterial and fungal lower than that of chloramphenicol and Nystatin, the reference drug.

Conclusions

A PDBO has been synthesized and characterized by combined experimental and theoretical quantum chemical calculations using B3LYP/6-31G(d,p) and B3LYP/6-311+g(d,p) basis set. By comparing calculated electronic transitions, chemical shifts and wavenumbers values with experimental value, it have been observed that B3LYP/6-311+G(d,p) estimate better results. NBO analysis investigation indicates the various types of interactions within molecule. A combined theoretical and experimental symmetric ($3319, 3320 \text{ cm}^{-1}$) and asymmetric ($3389, 3382 \text{ cm}^{-1}$) stretching wave number analysis confirms free NH_2 groups in the solid phase of PDBO. Topological parameters have been analyzed by Bader's 'Atoms in molecules' AIM theory and provide the existence of intramolecular hydrogen bonding ($\text{N-H} \cdots \text{O}$). The first hyperpolarizability (β_0) of the title compound is calculated as 23.83×10^{-30} esu indicates that PDBO is suitable for NLO applications. The preliminary bioassay suggested that the PDBO compound exhibits relatively good antibacterial and fungicidal activity against *E. coli*, *P. aeruginosa*, *S. aureus*, *S. pyogenes*, *C. albicans*, *A. niger*. The local reactivity descriptors analyses have been used to determine the reactive sites within molecule.

Acknowledgments

The authors are thankful to the DST and CSIR for providing research fund and IIT Kanpur for spectral data.

Appendix A. Supplementary data

Supplementary data associated with this article can be found, in the online version, at <http://dx.doi.org/10.1016/j.saa.2014.12.080>.

References

- [1] R.A. Lal, D. Basumatary, *Transition Metal Chem.* 32 (2007) 481–493.
- [2] V.P. Singh, P. Gupta, *Pharma. Chem. J.* 42 (2008) 180–196.
- [3] V.P. Singh, S. Singh, D.P. Singh, K. Tiwari, M. Mishra, *J. Mol. Struct.* 1058 (2014) 71–78.
- [4] Y.P. Wu, E. Rahm, R. Holze, *Electrochim. Acta* 47 (2002) 3491–3507.
- [5] M. Koh, T. Nakajima, R.N. Singh, *Mol. Cryst. Liq. Cryst.* 310 (1998) 341–346.
- [6] V.P. Gupta, P. Tandon, P. Rawat, R.N. Singh, A. Singh, *Astron. Astrophys.* 528 (2011) 129–134.
- [7] M.S.S. Adam, *Monatshchemie* 145 (2014) 435–445.
- [8] R.A. Lal, S. Choudhury, A. Ahmed, R. Borthakur, M. Asthana, A. Kumar, *Spectrochim. Acta Part A* 75 (2010) 212–224.
- [9] R.A. Lal, *Polyhedron* 8 (1989) 12519–12527.
- [10] V. Mimaite, J.V. Grazulevicius, J. Ostrauskaite, V. Jankauskas, *Dyes Pigm.* 95 (2012) 47–52.
- [11] T. Sedaghat, M. Aminian, G. Bruno, H.A. Rudbari, *J. Organomet. Chem.* 737 (2013) 26–31.
- [12] S. Ianelli, M. Nardelli, C. Pelizzi, *Gazz. Chim. Ital.* 115 (1985) 375.
- [13] R. Alonso, E. Bermejo, R. Carballo, A. Castineiras, T. Perez, *J. Mol. Struct.* 606 (2002) 153–173.
- [14] B.B. Safoklov, E.G. Atovmyan, L.A. Nikonova, *Russ. Chem. Bull.* 51 (2002) 2224–2229.
- [15] S.M.S.V. Wardell, M.V.N. De Souza, J.L. Wardell, *Acta Crystallogr. C* 62 (2006) 047–049.
- [16] A. Bacchi, A. Bonardi, M. Carcelli, P. Mazza, P. Pelagatti, C. Pelizzi, G. Pelizzi, C. Solinas, *J. Inorg. Biochem.* 69 (1998) 101–112.
- [17] L.D. Popov, S.I. Levchenkov, I.N. Shcherbakov, M.A. Kiskin, N.E. Borisova, A.A. Tsaturyan, V.A. Kogan, *J. Struct. Chem.* 54 (2013) 592–597.
- [18] P. Rawat, R.N. Singh, *Arabian J. Chem.* (2014), <http://dx.doi.org/10.1016/j.arabj.2014.10.050>.
- [19] Y. Shi, *Science* 288 (2002) 119–122.
- [20] G.J. Gainsford, M.D.H. Bhuiyan, A.J. Kay, *Acta. Crystallogr. Sect. E* 70 (2014) 029–030.
- [21] Y.V. Pereverzev, O.V. Prezhdo, L.R. Dalton, *Chem. Phys. Lett.* 37 (2003) 207–212.
- [22] C. Dehu, F. Meyers, J.L. Bredas, *J. Am. Chem. Soc.* 115 (1993) 6198–6208.
- [23] R.F.W. Bader, *Atoms in Molecule: A Quantum Theory*, Oxford University Press, Oxford, 1990, pp. 120–152.
- [24] V.A. Knizhnikova, N.E. Borisovab, N. Ya, L. Yurashevicha, L.A. Popovaa, A.Yu. Chernyadevc, Z.P. Zubreichuka, M.D. Reshetovab, *Russ. J. Org. Chem.* 43 (2007) 855–860.

- [25] M.J. Frisch et al., Gaussian 03 (Revision A.9), Gaussian Inc, Pittsburgh, 2003.
- [26] A.D. Becke, *J. Chem. Phys.* 98 (1993) 5648–5652.
- [27] C.T. Lee, W.T. Yang, R.G.B. Parr, *Phys. Rev.* 37 (1988) 785–790.
- [28] Computer program Gauss View 3.09, Ver. 2: Gaussian Inc, PA, Pittsburgh.
- [29] P. Pulay, G. Fogarasi, F. Pang, J.E. Boggs, *J. Am. Chem. Soc.* 10 (1979) 2550.
- [30] J.M.L. Martin, V. Alsenoy, C.V. Alsenoy, Gar2ped, University of Antwerp, 1995.
- [31] R.F.W. Bader, J.R. Cheeseman, in: AIMPAC Ed., 2000.
- [32] V. Cody, *Environ. Health Perspect.* 61 (1985) 163–183.
- [33] J.A. Paixao, M.R. Silva, A.M. Beja, A.J.F.N. Sobral, S.H. Lopes, A.M.d.A.R. Gonsalves, *Acta Cryst. E* 59 (2003) 094–096.
- [34] W.-N. Wu, X.-X. Li, Q.-F. Wang, Y.-W. Li, *Acta Cryst. E* 66 (2010) o2309.
- [35] R.N. Singh, P. Rawat, *J. Mol. Struct.* 1054–1055 (2013) 65–75.
- [36] B.B. Safoklov, E.G. Atovmyan, L.A. Nikonova, V.V. Tkachev, S.M. Aldoshin, *Russ. Chem. Bull.* 51 (2002) 2224–2229.
- [37] R.N. Singh, A. Kumar, R.K. Tiwari, P. Rawat, V.P. Gupta, *J. Mol. Struct.* 1035 (2013) 427–440.
- [38] S. Annamalai, A. Chinnadurai, *Anal. Methods* (2014), <http://dx.doi.org/10.1039/C4AY00653D>.
- [39] F. Weinhold, C.R. Landis, *Valency and Bonding: A Natural Bond Orbital Donor–Acceptor Perspective*, Cambridge University Press, Cambridge, New York, Melbourne, 2005. pp. 215–274.
- [40] R.G. Parr, W. Yang, *Functional Theory of Atoms and Molecules*, Oxford Univ. Press, NY, 1989.
- [41] P. Geerlings, F. De Proft, W. Langenaeker, *Chem. Rev.* 103 (2003) 1793–1873.
- [42] P. Rawat, R.N. Singh, *J. Mol. Struct.* 1074 (2014) 201–212.
- [43] P. Rawat, R.N. Singh, *J. Mol. Struct.* 1075 (2014) 462–470.
- [44] R.N. Singh, A. Kumar, R.K. Tiwari, P. Rawat, R. Manohar, *Struct. Chem.* 24 (2013) 713–724.
- [45] R.N. Singh, A. Kumar, R.K. Tiwari, P. Rawat, *Spectrochim. Acta Part A* 112 (2013) 182–190.
- [46] R.N. Singh, A. Kumar, R.K. Tiwari, P. Rawat, *Spectrochim. Acta Part A* 113 (2013) 378–385.
- [47] P. Rawat, R.N. Singh, *J. Mol. Struct.* 1081 (2015) 293–303.
- [48] R.N. Singh, P. Rawat, S. Sahu, *J. Mol. Struct.* 1054–1055 (2013) 123–133.
- [49] R.N. Singh, A. Kumar, R.K. Tiwari, P. Rawat, *J. Mol. Struct.* 1035 (2013) 295–306.
- [50] R.N. Singh, P. Rawat, S. Sahu, *J. Mol. Struct.* 1076 (2014) 437–445.
- [51] R.N. Singh, P. Rawat, A. Kumar, *J. Mol. Struct.* 1061 (2014) 140–149.
- [52] R.S. Mulliken, *J. Chem. Phys.* 2 (1934) 782–793.
- [53] T.A. Koopmans, *Physica* 1 (1933) 104–113.
- [54] R.N. Singh, P. Rawat, S. Sahu, *Spectrochim. Acta Part A* 135 (2015) 1162–1168.
- [55] N.R. Babu, S.S.C. Bose, M.S. Ali Padusha, H. Saleem, Y. Erdođdu, *Spectrochim. Acta A* 120 (2014) 314–322.
- [56] F. Guégan, P. Mignon, V. Tognetti, L. Joubert, C. Morell, *Phys. Chem. Chem. Phys.* (2014), <http://dx.doi.org/10.1039/C4CP01613K>.
- [57] N. Sukumar, *A Matter of Density: Exploring the Electron Density Concept in the Chemical, Biological, and Materials Sciences*, Wiley-Blackwell, 2012.
- [58] O. Christiansen, J. Gauss, J.F. Stanton, *Chem. Phys. Lett.* 305 (1999) 147–155.
- [59] Ana E. De A. Machado¹, L.A. Ana, H.F. Dos Santos, Wagner B. De Almeida, *J. Polym. Sci. Part B: Polym. Phys.* 49 (2011) 1410–1419.
- [60] P. Rawat, R.N. Singh, *J. Mol. Struct.* 1082 (2015) 118–130.
- [61] A.E. Whitten, P. Turner, W.T. Klooster, R.O. Piltz, M.A. Spackman, *J. Phys. Chem. A* 110 (2006) 8763–8776.
- [62] J.L. Oudar, D.S. Chemla, *J. Chem. Phys.* 66 (1977) 2664–2668.